INTERNATIONAL JOURNAL FOR NUMERICAL METHODS IN ENGINEERING
Int. J. Numer. Meth. Engng. 2000; **48**:37–53

Study of shrinkage stresses for drying of brick as a conjugate problem

K. Murugesan[1], K. N. Seetharamu[2,‡], P. A. Aswatha Narayana[3,‡], H. R. Thomas[4,*,†,§] and W. J. Ferguson[5]

[1] *Department of Mechanical Engineering, KREC, Surathkal, India*
[2] *Universiti Sains Malaysia, Perak Campus, Malaysia*
[3] *Fluid Mechanics Laboratory, IIT, Madras, India*
[4] *Geoenvironmental Research Centre, Cardiff School of Engineering, University of Wales, Cardiff, U.K.*
[5] *Department of Civil and Offshore Engineering, Heriot-Watt University, Edinburgh, U.K.*

SUMMARY

Drying induced shrinkage stresses of a two-dimensional rectangular brick of aspect ratio 2 is studied numerically. The drying of brick is analysed as a conjugate problem. The conservation equations for the solid are obtained using continuum approach and the Navier–Stokes equations have been solved for the flow field. An elastic model has been used to calculate the shrinkage stresses. The present unified model predicts the stress concentration at the leading edge where it is expected to be maximum due to large shrinkage. Copyright © 2000 John Wiley & Sons, Ltd.

KEY WORDS: conjugate drying; material shrinkage; stress distribution; elastic stress

INTRODUCTION

The binder removal process from wet pressed clay products such as tiles, bricks, electrical insulators, etc., is considered to be a very critical process. These products, which are in their final shape, have to be dried to their equilibrium moisture contents, without causing damage to their shape and size. Evaporation of water from such products results in shrinkage. If uneven shrinkage takes place during drying, shrinkage stresses will be developed, leading to the formation of crack or warping.

Also, the stress–strain variations during drying is affected by the drying behaviour of the material. Hence a knowledge about the drying induced stress is very important in order to prevent damage to the products.

* Correspondence to: H. R. Thomas, School of Engineering, University of Wales, College of Cardiff, P.O. Box 925, Cardiff CF2 IYF, U.K.
† E-mail: thomashr@cardiff.ac.uk
‡ Professor
§ Director

Received 7 October 1998
Revised 13 July 1999

The moisture movement within the solid during drying may be due to capillary forces during the constant rate drying period or due to diffusion during the falling rate period [1]. These different regimes of drying have been studied theoretically with the help of one- [2, 3] and two-dimensional [4, 5] models using heat and mass transfer coefficients from the available boundary layer correlations. Christian Dietl *et al.* [6] developed a model for the drying of porous solid based on the conservation of heat and enthalpy flow rates as well as mass flow rates for differential control volume. An inverse procedure was developed to determine the moisture conductivity and vapour resistance of the solid, by utilizing experimentally obtained drying curves. Numerical results were obtained for the drying of concrete, brick, clay, wheat and pine and were compared with their experimental results. The drying of solid along with the drying medium has also been studied as a conjugate problem for both natural convection [7] and forced convection cases [8, 9].

The drying induced stresses in a brick was studied by Nikitenko *et al.* [10] using thermoplasticity equations. Deformations have been described only by normal strains and it has been found that reducing the moisture removal at large faces and increasing the moisture removal at the small faces of the brick can result in a reduction in the maximum generalized stress for a constant drying time. Lewis *et al.* [11] used Luikov's equations for the solid to determine the temperature and moisture distributions in brick, timber and ceramic insulator. They used heat and mass transfer coefficients from standard correlations. Initially, they used an elastic model to calculate the stresses. Later Lewis *et al.* [12] improved their model by considering an elasto-viscoplastic model for stress analysis. They found that when the outside layers of the brick dry faster than the layers inside, the solid tends to shrink onto the wet inner core and gives rise to tensile stresses on the outerlayers and compressive stresses at the centre.

Takao *et al.* [13] derived an elasto-plastic model based on virtual work principle to study the stresses induced during drying of hydrated starch granules. The total strain was calculated by adding the free strain due to moisture removal and strain due to deformation described by the material law. Collard *et al.* [14] studied the stress developed during convective drying of a clay plate. The stress–strain relationship was considered to follow the elastic/viscoplastic behaviour with Mohr–Coulomb yield criterion. The rheological parameters are functions of moisture content which were determined from experiments. Ferguson [15] studied the effects of airflow and wet bulb temperature on stress development during convective drying of timber boards. The total strain comprises elastic strain, free shrinkage strain and a strain due to mechano-sorptive creep. His results show that increasing the airstream velocity does not produce a marked change in the maximum tensile stress. Also he found that by reducing the wet bulb depression, the maximum tensile stress decreases. Kowalski *et al.* [16] studied the drying induced deformation and stresses for clay products. The governing equations for the drying problem and the stress problem were solved using finite element method. The effect of change in humidity and temperature of the drying medium on the deformation and stresses were studied in order to control the drying processes to avoid stresses that cause fracture. They found that the alterations in both the temperature and humidity of the drying medium allow for stress reduction.

In the earlier works, the heat and mass transfer coefficient values at the interface of the solid are specified from standard correlations. Also, these coefficients were assumed to be constant throughout the solid surfaces. Numerical results with constant heat and mass transfer coefficient values indicate uniform shrinkage of the solid over the surfaces. But in reality, drying of brick is a conjugate problem. Leading edge dries faster when compared to other surfaces and the

shrinkage over the surfaces will not be uniform. Hence, the drying of brick has to be studied along with the flow field as a conjugate problem. The moisture evolutions obtained from such analysis has to be used to obtain the shrinkage stress distributions within the solid.

In the present work, a unified approach has been followed to study the drying induced shrinkage stresses along with the flow field. The two-dimensional Navier–Stokes equations have been solved for the flow field, which will enable one to study the conjugate drying of any two-dimensional shape like brick, tile, etc. Using the moisture evolutions obtained from the conjugate analysis, strains are calculated. For simplicity, only an elastic model has been used to calculate the stresses since emphasis is on the development of an unique model to take care of the flow field and the shrinkage stresses. Drying results have been obtained for a brick having an aspect ratio 2 for the initial drying period where the solid approaches the constant drying period. Since the maximum shrinkage occurs [16] during this period results were obtained to determine the maximum stress due to the leading edge effect.

MATHEMATICAL MODEL

The drying of a rectangular brick of aspect ratio 2, saturated with water is considered for the analysis. Air is assumed to flow over the brick with uniform velocity. The moisture transfer from the solid takes place due to the concentration potential difference between the solid surface and the drying medium. This causes the solid to lose some sensible heat, resulting in a decrease in temperature. The evaporation of moisture results in the shrinkage of the brick. Since the leading edge dries faster, more shrinkage is expected at the leading edge compared to the other sides of the solid. Knowing the amount of moisture evaporated, the strain induced in the brick can be determined. Using an elastic model, the stress distributions within the brick are calculated.

GOVERNING EQUATIONS

The conservation equations for the porous solid are obtained using continuum approach. Two-dimensional Navier–Stokes equations, energy and concentration equations are solved for the flow field. Simple elastic model has been used to calculate the stress distribution within the solid during drying. Conjugate drying of a rectangular brick is treated as a plane strain problem.

POROUS SOLID

The two-dimensional conservation equations for liquid and vapour in the porous solid can be obtained as follows using the species equations [3]:

Liquid:

$$\frac{\partial w_{\mathrm{l}}}{\partial t} = -\frac{1}{\rho_0}\left[\frac{\partial J_{\mathrm{lx}}}{\partial x} + \frac{\partial J_{\mathrm{ly}}}{\partial y}\right] + \frac{\dot{m}}{M_0} \tag{1}$$

Vapour:

$$\frac{\partial w_v}{\partial t} = -\frac{1}{\rho_0}\left[\frac{\partial J_{vx}}{\partial x} + \frac{\partial J_{vy}}{\partial y}\right] - \frac{\dot{m}}{M_0} \tag{2}$$

where J is the diffusion flux of moisture and w is the moisture content per kg of dry solid.

Energy equation for liquid and vapour in the solid is written as follows:

$$\rho_0 \frac{\partial}{\partial t}(\sum w_j H_j) = \frac{\partial}{\partial x}\left(k\frac{\partial T}{\partial x}\right) + \frac{\partial}{\partial y}\left(k\frac{\partial T}{\partial y}\right) - \frac{\partial}{\partial x}(\sum J_j H_j) - \frac{\partial}{\partial y}(\sum J_j H_j) \tag{3}$$

where j represents liquid or vapour.

During the initial period of drying, the moisture (liquid) movement will be due to capillary forces and during the later part of drying, the moisture movement (vapour) is due to diffusion. Hence, the moisture transport within the solid can be represented as sum of fluxes due to capillary forces and due to diffusion. As pointed out by Kallel *et al.* [3], the different drying regimes can be represented by a single equation using the above approach. Hence using Darcy's law for liquid movement and Fick's law for vapour diffusion, Equations (1) and (2) can be written as follows:

$$\frac{\partial w_l}{\partial t} = \frac{\partial}{\partial x}\left[D_{ml}\frac{\partial W}{\partial x} + D_{Tl}\frac{\partial T}{\partial x}\right] + \frac{\partial}{\partial y}\left[D_{ml}\frac{\partial W}{\partial y} + D_{Tl}\frac{\partial T}{\partial y}\right] + \frac{\dot{m}}{M_0} \tag{4}$$

$$\frac{\partial w_v}{\partial t} = \frac{\partial}{\partial x}\left[D_{mv}\frac{\partial W}{\partial x} + D_{Tv}\frac{\partial T}{\partial x}\right] + \frac{\partial}{\partial y}\left[D_{mv}\frac{\partial W}{\partial y} + D_{Tv}\frac{\partial T}{\partial y}\right] - \frac{\dot{m}}{M_0} \tag{5}$$

where D_{ml}, D_{Tl}, D_{mv}, D_{Tv} represent the isothermal and non-isothermal coefficients obtained after simplifications of the moisture conservation equations for liquid and vapour. These coefficients are defined in such a way that the moisture transport within the solid is represented in the form of a diffusion equation. They are strong functions of moisture content of the solid and the relative magnitudes of the coefficients for liquid and vapour represent the predominant nature of capillary effect during the initial period of drying and diffusion in the later part of drying.

The rate of vapour condensation, $\dot{m}/M_0$ can be obtained from Equations (4) and (5) as follows:

$$\frac{\dot{m}}{M_0} = \frac{\partial}{\partial x}\left[D_{mv}\frac{\partial w_l}{\partial x} + D_{Tv}\frac{\partial T}{\partial x}\right] + \frac{\partial}{\partial y}\left[D_{mv}\frac{\partial w_l}{\partial y} + D_{Tv}\frac{\partial T}{\partial y}\right] \tag{6}$$

Since $w_v \ll w_l$, the final form of the moisture conservation equation can be obtained from the summation of Equations (4) and (5) as follows:

$$\frac{\partial W}{\partial t} = \frac{\partial}{\partial x}\left[(D_{mv} + D_{ml})\frac{\partial W}{\partial x} + (D_{Tv} + D_{Tl})\frac{\partial T}{\partial x}\right] + \frac{\partial}{\partial y}\left[(D_{mv} + D_{ml})\frac{\partial W}{\partial y} + (D_{Tv} + D_{Tl})\frac{\partial T}{\partial y}\right] \tag{7}$$

The convective term in the energy equation is very small when compared to the diffusion and phase change terms [3]. Hence by dropping the convective term from the energy equation (3), the final form of the energy equation for the solid can be written as follows:

$$C^* \frac{\partial T}{\partial t} = \frac{1}{\rho_0}\left[\frac{\partial}{\partial x}\left(k\frac{\partial T}{\partial x}\right) + \frac{\partial}{\partial y}\left(k\frac{\partial T}{\partial y}\right)\right] + \frac{\dot{m}}{M_0}(H_v - H_l) \tag{8}$$

where the equivalent specific heat capacity for the porous solid is determined as

$$C^* = C_0 + w_l C_l + w_v C_v$$

Equations (7) and (8) are the final forms of the mass and energy transport equations for the porous solid. These equations are non-linear and coupled.

GOVERNING EQUATIONS FOR THE FLOW FIELD

The two-dimensional Navier–Stokes, energy and concentration equations are considered as follows:

Continuity:

$$\frac{\partial u}{\partial x} + \frac{\partial v}{\partial y} = 0 \tag{9}$$

x-momentum:

$$\frac{\partial u}{\partial t} + u\frac{\partial u}{\partial x} + v\frac{\partial u}{\partial y} = -\frac{1}{\rho_0}\frac{\partial p}{\partial x} + \frac{\mu}{\rho_f}\left[\frac{\partial^2 u}{\partial x^2} + \frac{\partial^2 u}{\partial y^2}\right] \tag{10}$$

y-momentum:

$$\frac{\partial v}{\partial t} + u\frac{\partial v}{\partial x} + v\frac{\partial v}{\partial y} = -\frac{1}{\rho_0}\frac{\partial p}{\partial y} + \frac{\mu}{\rho_f}\left[\frac{\partial^2 v}{\partial x^2} + \frac{\partial^2 v}{\partial y^2}\right] \tag{11}$$

Energy equation:

$$\frac{\partial T}{\partial t} + u\frac{\partial T}{\partial x} + v\frac{\partial T}{\partial y} = \frac{k}{\rho_f C_{pf}}\left[\frac{\partial^2 T}{\partial x^2} + \frac{\partial^2 T}{\partial y^2}\right] \tag{12}$$

Concentration equation:

$$\frac{\partial C}{\partial t} + u\frac{\partial C}{\partial x} + v\frac{\partial C}{\partial y} = D\left[\frac{\partial^2 C}{\partial x^2} + \frac{\partial^2 C}{\partial y^2}\right] \tag{13}$$

The interfacial boundary conditions for the porous solid and the drying medium are given as follows:

No slip:

$$u = 0, \quad v = 0 \tag{14}$$

Temperature continuity:

$$T_{\mathrm{f}} = T_{\mathrm{s}} \tag{15}$$

Concentration continuity:

$$C_{\mathrm{f}} = C(T, W)_{\mathrm{s}} \tag{16}$$

Heat balance:

$$[k + \rho_0 (H_{\mathrm{v}} - H_{\mathrm{l}}) D_{T\mathrm{v}}] \frac{\partial T}{\partial n} + \rho_0 (H_{\mathrm{v}} - H_{\mathrm{l}}) D_{m\mathrm{v}} \frac{\partial W}{\partial n} = k_{\mathrm{f}} \frac{\partial T_{\mathrm{f}}}{\partial n} + \rho_0 (H_{\mathrm{v}} - H_{\mathrm{l}}) D \frac{\partial C_{\mathrm{f}}}{\partial n} \tag{17}$$

where D is the diffusion coefficient for vapour in the drying medium.

Species flux balance

$$\rho_0 \left[D_{T\mathrm{v}} \frac{\partial T}{\partial n} + D_{m\mathrm{v}} \frac{\partial W}{\partial n} \right] = D \frac{\partial C_{\mathrm{f}}}{\partial n} \tag{18}$$

The gas-phase boundary conditions are:

At inlet ($x = 0$), $u = U_\alpha$, $v = 0$, $T = T_\alpha$ and $C = C_\alpha$.
In the far stream ($y = H_{\mathrm{f}}$), $u = U_\alpha$, $T = T_\alpha$ and $C = C_\alpha$.

The bottom boundary is taken as adiabatic for both heat and mass transfer and smooth extrapolation is used at the outlet flow boundary ($x = L_{\mathrm{f}}$).

STRESS ANALYSIS

The drying induced stresses are calculated as an initial strain problem. The stress vector can be written in terms of the initial strains and elasticity matrix as follows:

$$\{\sigma\} = [D] (\{e\} - \{e_0\}) \tag{19}$$

where $[D]$ is the elasticity matrix given by

$$[D] = \frac{E(1-\gamma)}{(1+\gamma)(1-2\gamma)} \begin{bmatrix} 1 & \dfrac{\gamma}{(1-\gamma)} & 0 \\ \dfrac{\gamma}{(1-\gamma)} & 1 & 0 \\ 0 & 0 & \dfrac{(1-2\gamma)}{2(1-2\gamma)} \end{bmatrix} \tag{20}$$

$\{e\}$ is the strain vector and e_0 is the initial strain due to shrinkage.

The strains can be written in the matrix form in terms of displacements and $[B]$ matrix as

$$e = \begin{Bmatrix} e_x \\ e_y \\ e_{xy} \end{Bmatrix} = \begin{Bmatrix} \dfrac{\partial u}{\partial x} \\ \dfrac{\partial v}{\partial y} \\ \dfrac{\partial u}{\partial y} + \dfrac{\partial v}{\partial x} \end{Bmatrix} \tag{21}$$

and

$$e = [B]\ \{\delta\}^e \tag{22}$$

where

$$[B] = [B_i\ \ B_j\ \ B_k]$$

and

$$B_i = \begin{Bmatrix} b_i & 0 \\ 0 & c_i \\ c_i & b_i \end{Bmatrix}$$

$$\{\delta\} = \begin{Bmatrix} u_i \\ v_i \\ u_j \\ v_j \\ u_k \\ v_k \end{Bmatrix}$$

In the above expression for δ, $u_i, v_i, u_j, v_j, u_k, v_k$ are the nodal displacements in the x and y directions at i, j and k nodes of an element and b_i, c_i are constants used with B matrix for linear triangular elements [17].

Finally, the stress vector is given by the following equation as

$$\{\sigma\} = [D][B]\{\delta\} - [D]\{e_0\} + \sigma_0 \tag{23}$$

where σ_0 is the initial residual stress present in the material.

NUMERICAL SOLUTION PROCEDURE

The Galerkin's weighted residual method has been used to integrate the governing equations (7)–(13). Triangular elements are used to represent the variables in the above governing equations. Within each element, the variables are represented in terms of their nodal values using the following expression:

$$\phi = N_i \phi_i + N_j \phi_j + N_k \phi_k$$

where ϕ is any flow or transport variable and N_i, N_j and N_k are the nodal shape functions.

SOLUTION PROCEDURE FOR THE FLOW FIELD

The flow field has been solved using Eulerian velocity correction method. The algorithm has the following steps [18]:

(i) calculation of pseudo-velocities, neglecting the pressure terms in the x and y momentum equations,
(ii) evaluation of pressure from pressure Poisson equation and
(iii) correction of the pseudo velocities to get actual velocities.

Since the characteristic time scale of the flow field is much smaller compared to the time scale of the heat and moisture transfer within the porous solid [8], the flow field is assumed to be in a steady-state condition for the entire drying period.

CONJUGATE SOLUTION PROCEDURE

The solution of the governing equations (7)–(13) are obtained using the boundary conditions given by Equations (14)–(18) and the steps are as follows:

(i) The solution of the flow equations (9)–(11) are obtained using the Eulerian velocity correction method.
(ii) Using these velocities, the transient solution of the energy and concentration Equations (12) and (13) are obtained using dirichlet boundary conditions.

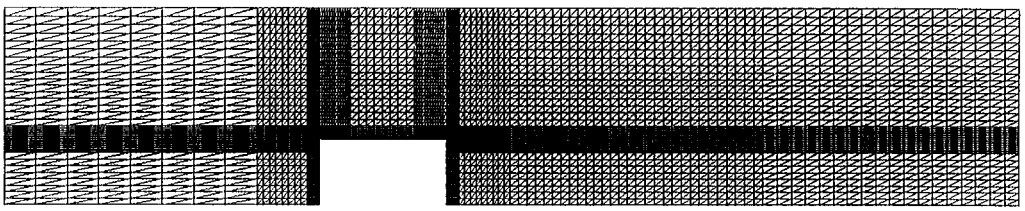

Figure 1. Computational mesh.

(iii) Using a five-point fit, the gradients of temperature and concentration at the surface of the solid are calculated. Then the heat and mass flux at the interface of the solid are determined using these gradients and thermal conductivity and diffusion coefficient of the drying medium.

(iv) The mass concentration of the flow field at the interface (Equation (16)) is calculated with the local relative humidity. The local relative humidity is calculated using Henderson's modified equation for desorption isotherm [19] which is given as

$$\phi = 1 - \exp(-17\,W^{0.6})$$

The constants in the above equation are obtained by trial and error to satisfy the equilibrium moisture content of the brick at 50 per cent relative humidity.

(v) Using the fluxes, the conservation equations (7) and (8) of the porous solid are solved to obtain the temperature and moisture content within the solid.

(vi) The temperature and moisture content at the surface of the solid are then changed.

(vii) Knowing the change in the moisture content of the entire solid, the average moisture content of the solid is determined.

(viii) By comparing the moisture content in every element of the solid at a given time, with the moisture content in the corresponding element at the previous time step, the strains in the elements are calculated.

(ix) Knowing the strains in the elements the stresses are calculated using the relationship for an elastic model [20].

Steps (ii)–(ix) are repeated for the next time step and the temperature and concentration within the flow field, temperature and moisture content within the solid and the strains and stresses induced in the solid are thus calculated with time. Based on a grid sensitivity analysis, the number of nodes and elements used for the solid and flow domains are 531 and 1024; 4465 and 8576, respectively. The final mesh used for the computations is shown in Figure 1. The CPU time taken for simulating 1 h of drying process with stress calculation, is 8 h on an IBM - RS 6000 machine.

RESULTS AND DISCUSSION

Detailed experimental results are not available for validating the simulation of drying of brick as a conjugate problem. Therefore, the different modules of the unified code has been validated

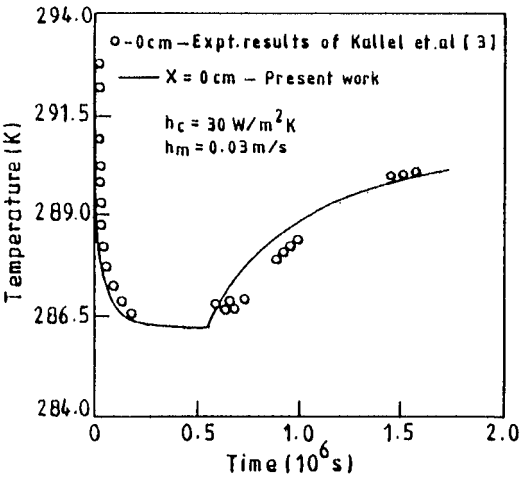

Figure 2. Experimental comparison of 1-D results.

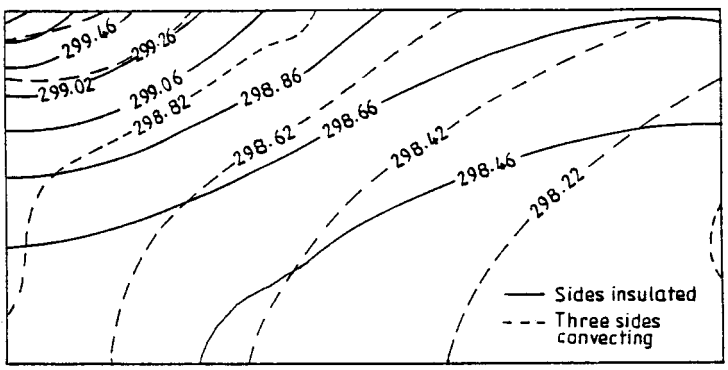

Figure 3. Comparison of temperature contours at 2 h for timber drying analysis at Re = 200 [$T_i = 298$ K, $T_\alpha = 333$ K, $W_i = 0.45$, $\phi = 10$ per cent].

separately. The flow code has been verified with the results of Chien-Tung Yang and Satya [21] for two-dimensional flow over a square block. One-dimensional experimental results are available for brick drying [3]. The two-dimensional solid model has been used to simulate the one-dimensional results by setting adiabatic conditions on the side surfaces. The simulated results are compared with the experimental results of Kallel *et al.* [3] as shown in Figure 2. The conjugate drying of wood has been studied by Oliveira and Haghighi [9] using boundary layer equations for the flow field for Re = 200. The same problem has been simulated in the present study by setting the sides of the brick adiabatic. The temperature and moisture contours obtained by the present work are compared with those predicted by Oliveira and Haghighi and are shown in Figures 3 and 4. Though our simulation results agree qualitatively with those of Oliveira and

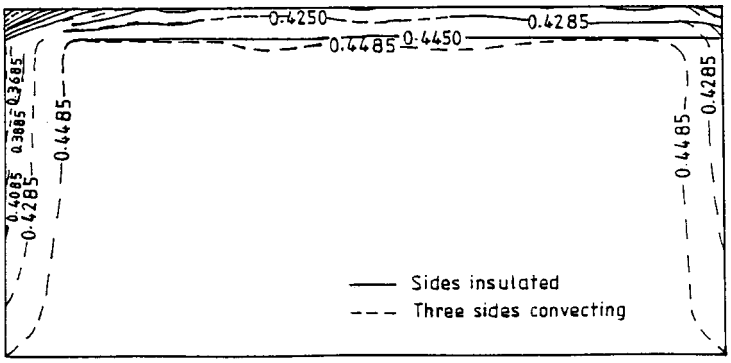

Figure 4. Comparison of moisture contours at 2 h for timber drying.

Haghighi [9], the quantitative comparison has not been obtained, because all the transport properties of wood, required for the present model are not available.

DRYING OF BRICK

The schematic diagram of the computational domains for the conjugate drying problem is shown in Figure 5. Points A, B, C and D represent the corners of the brick. The drying medium (air) is assumed to flow with a velocity of 1.8 m/min (equivalent to Reynolds number of 200 based on the height of brick, 0.1 m) at a temperature of 293.0 K and with 50 per cent relative humidity. The solid is assumed to be at the same temperature of air and saturated with moisture of 0.13 kg/kg of dry solid. Due to the concentration difference between the solid surface and the ambient, evaporation takes place initially at the solid surface. Since there is no other source of heat supply, the heat of vaporization is absorbed initially from the solid itself. Hence the temperature at the solid surface decreases. With drop in temperature at the solid surface, convective heat transfer takes place from the ambient to the solid. Hence for further evaporation, the heat absorbed from the solid decreases. When the equilibrium is reached between the heat of vaporization and the heat supply from the ambient, the solid reaches the wet bulb temperature corresponding to the ambient conditions. The temperature of the solid remains constant at this temperature for some time and then the temperature increases due to the convective heat transfer from the ambient.

The temperature distribution along the length of the brick, at the end of 1 h is shown in Figure 6. The drop in temperature at the leading edge B is always higher than the values at the other surfaces, since the thickness of boundary layer is very thin at the leading edge. Corner A is in the upstream stagnation zone and corner D in the recirculation zone. The convective resistance for heat and mass transfer will be high in these regions. Hence the evaporation from corners A and D are very less compared to corner B. The leading edge effects are also observed in moisture distributions as shown in Figure 7. The temperature and concentration distributions in the gas phase at the end of 36 h, are shown in Figures 8 and 9, respectively. The figures illustrate that after the establishment of the boundary layers, the changes in heat and mass transfer processes are rather slow. However, the temperature field evolves relatively faster than the

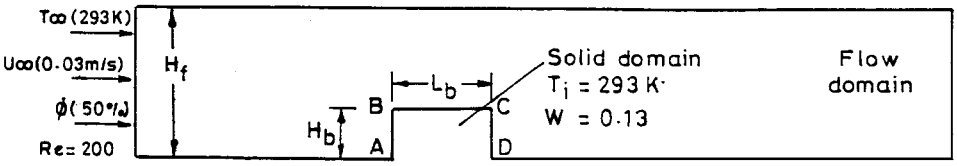

Figure 5. Schematic diagram of computational domains.

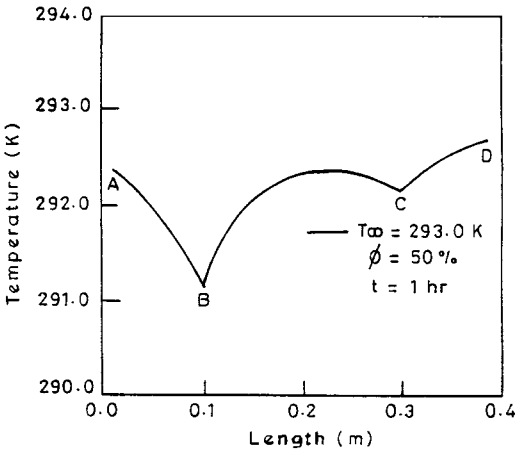

Figure 6. Temperature distribution along the surface of the brick.

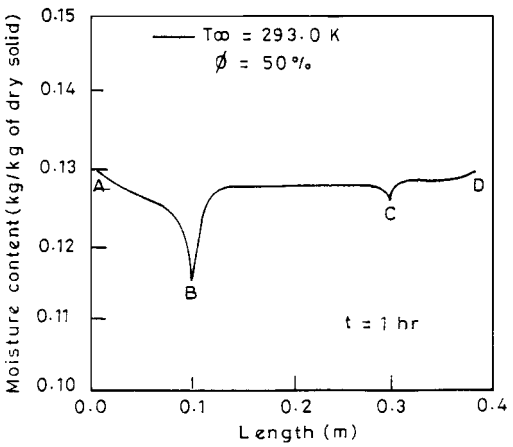

Figure 7. Moisture distribution along the surface of the brick.

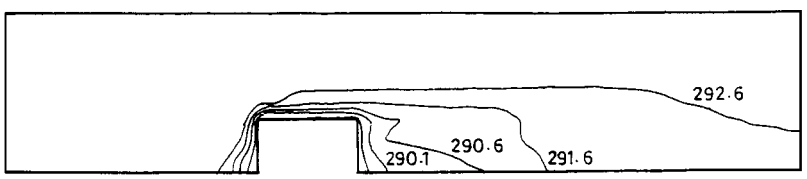

Figure 8. Temperature (K) contours in the flow field at the end of 36 h.

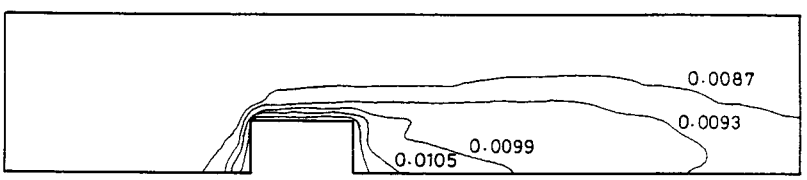

Figure 9. Concentration (kg/m^3) contours in the flow field at the end of 36 h.

moisture concentration field. It is also evident that while the bulk of the heat and mass transfer occur through the top surface, the side surfaces also have limited contributions.

STRESS ANALYSIS

The moisture distribution within the solid is obtained using the conjugate model. Using these results, the strain induced within the solid is calculated. The solid shrinks due to evaporation. Figure 10 shows the shape of the rectangular brick after and before drying. The solid line indicates the shape of the brick after drying at the end of 3 h. The dotted line indicates the original shape of the brick before drying. It can be observed from the figure that the leading edge shrinkage is more compared to the other sides. Also, the left-hand side shrinks more compared to the right-hand side due to the leading edge effect. In order to bring out the effect of use of constant values of heat and mass transfer coefficients on shrinkage, drying results were obtained with constant values of heat and mass transfer coefficients over the surfaces. Using the moisture distributions for the above case, the shrinkage of the solid at the end of 1 h is shown in Figure 11. As seen from the figure, both the left-hand and right-hand sides shrink in the same proportion, because the evaporation from these sides are equal. But in reality the leading edge shrinks more due to the presence of thin boundary layer.

The principal stress distribution within the brick at the end of 3 h is shown in Figure 12 for conjugate drying results. The stress near the leading edge reaches a maximum of 55 MPa. Because

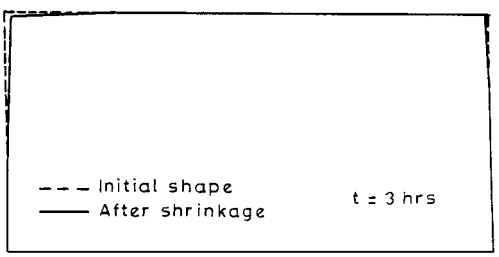

Figure 10. Shrinkage of brick at the end of 3 h for conjugate analysis.

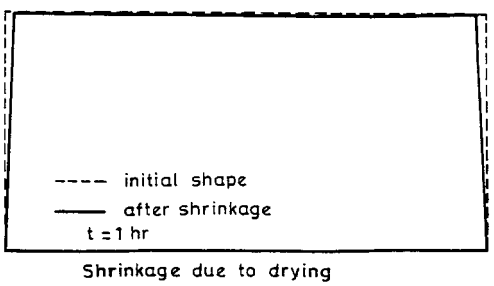

Figure 11. Shrinkage of brick at the end of 1 h for 2-D analysis.

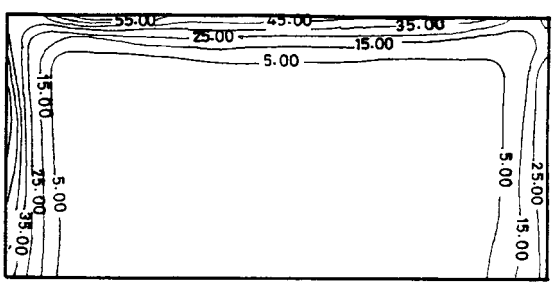

Figure 12. Principal stress contours at the end of 3 h for conjugate analysis.

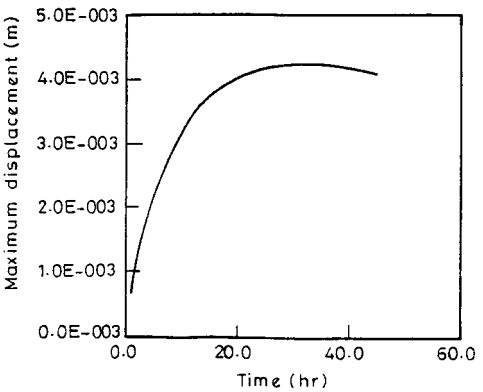

Figure 13. Variation of maximum displacement with time.

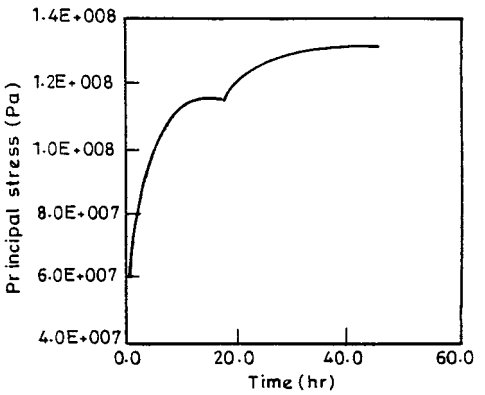

Figure 14. Variation of principal stress with time.

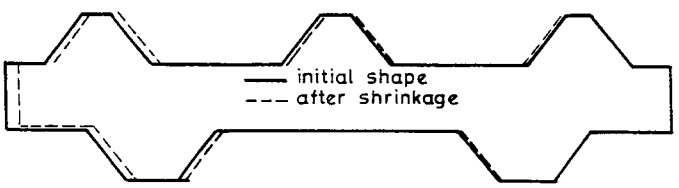

Figure 15. Shrinkage of roof tile at the end of 30 min.

the sides closer to the leading edge dries faster, resulting in more shrinkage compared to the other sides. The variation of maximum displacement during the drying is calculated for a period of 45 h using conjugate drying analysis and is shown in Figure 13. The maximum displacement increases with time as drying proceeds and reaches a maximum at the end of nearly 30 h. Afterwards the displacement shows a decreasing trend and the shrinkage will continue as long as the free water is removed from the brick. When the free water is completely removed, no further shrinkage will be observed by the removal of the remaining bound water. The variation of principal stress with time is shown in Figure 14. The stress increases initially and then decreases slightly at about 20 h. Because the effect of temperature gradient on evaporation decreases as the temperature gradient starts decreasing during this period. Henceforth, the shrinkage is mainly due to the evaporation by moisture gradient. That is why there is a slow rate of increase of principal stress beyond 20 h.

DRYING INDUCED STRESSES FOR A ROOF TILE

The moisture distribution within a roof tile of overall width 200 mm and height 50 mm, is obtained using constant values of heat and mass transfer coefficients over the sides of the tile. Using these drying results, the shrinkage of the tile is obtained and is shown in Figure 15. Non-uniform shrinkage of the tile is observed between the left-hand and the right-hand side

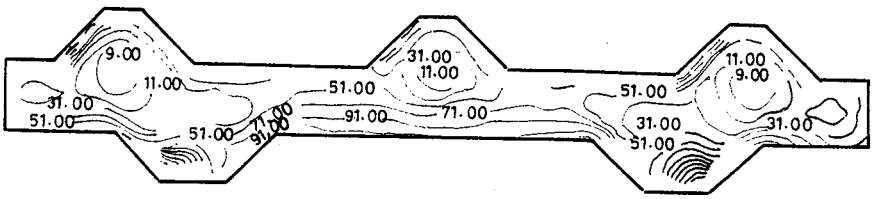

Figure 16. Principal stress contours for roof tile.

about the central axis, since the constraint points were considered only at the right-hand side of the tile, where the shrinkage is minimum. The distribution of principal stresses within the tile is shown in Figure 16. It can be observed from this figure that maximum stress occurs near the corners of the solid wherein the shrinkage is more. The stresses are more at sharp corners throughout the tile.

CONCLUSIONS

The study of conjugate drying along with drying induced stresses has been carried out for a rectangular brick of aspect ratio 2, using two-dimensional Navier–Stokes equations for the flow field and an elastic model for the stress analysis. The results indicate maximum stress occurring at the regions closer to the leading edge. Because of the two-dimensional effect of the solid, the boundary layer thickness vary over the sides of the solid, which shows that the resistance for heat and mass transfer over the surfaces of the solid is not constant. Hence, the shrinkage varies over the sides resulting in a non-uniform stress distribution over the sides of the solid. If proper control over the drying medium is not there, this may result in the formation of cracks. The drying induced stress results obtained for a roof tile indicates maximum stress concentration at the sharp corners of the tile.

APPENDIX: NOMENCLATURE

A = area normal to x or y direction (m^2)
B = gradient matrix
C = specific heat capacity (J/kg K); concentration (kg/m^3)
C^* = equivalent specific heat (J/kg K)
D = diffusion coefficient (m^2/s)
D_m = isothermal diffusion coefficient (m^2/s)
D_T = non-isothermal diffusion coefficient (m^2/s K)
e = strain
H = enthalpy (J/kg); height (m)
h_c = convective heat transfer coefficient (W/m^2 K)
h_m = convective mass transfer coefficient (m/s)
J = mass flux (kg/m^2 s)

k = thermal conductivity (W/m K)
L = length (m)
M = mass (kg)
$\dot{m}$ = rate of phase change (kg/s)
p = pressure (Pa)
Re = Reynolds number based on the height of brick (Re = $\rho UH/\mu$)
t = time (s)
T = temperature (K)
u = velocity in x direction (m/s)
v = velocity in y direction (m/s)
U_α = free stream velocity (m/s)
w = moisture content in liquid or vapour phase (kg/kg of dry solid)
W = total moisture content ($w_l + w_v$)
x, y = spatial coordinates

Greek letters

μ = coefficient of dynamic viscosity (Pa s)
ϕ = relative humidity
ρ = density (kg/m^3)
σ = stress (Pa)
γ = Poisson's ratio

Subscripts

b = brick
f = fluid or flow domain
i = initial conditions; node of an element
j = mobile component (liquid or vapour); node of an element
k = node of an element
l = liquid
o = dry solid
s = surface conditions
v = vapour
w = moisture (liquid or vapour)
α = ambient conditions

REFERENCES

1. Luikov AV. *Heat and Mass Transfer in Capillary Porous Bodies*. Pergamon Press: New York, 1966.
2. Huang CLD. Multi-phase moisture transfer in porous media subjected to temperature gradient. *International Journal of Heat and Mass Transfer* 1979; **22**:1295–1307.
3. Kallel F, Galanis N, Perrin B, Javelas R. Effects of moisture on temperature during drying of consolidated porous materials. *Journal of Heat Transfer, ASME Transactions* 1993; **115**:724–733.
4. Comimi G, Lewis RW. A numerical solution of two-dimensional problems involving heat and mass transfer. *International Journal of Heat and Mass Transfer* 1976; **19**:1387–1392.
5. Ferguson WJ, Lewis RW. A comparison of a fully non-linear and a partially non-linear heat and mass transfer analysis of a timber drying problem. *Proceedings of the VII International Conference on Numerical Methods in Thermal Problems*, vol. VII. Part 2, 1991; 973–984. Stanford.

6. Dietl Christian, Winter Edgar RF, Viskanta Raymond. An efficient simulation of the heat and mass transfer processes during drying of capillary, porous, hygroscopic materials. *International Journal of Heat and Mass Transfer* 1998; **41**:3611–3625.
7. Zeghmati B, Daguenet M. Study of laminar free convection over an inclined wet flat plate. *International Journal of Heat and Mass Transfer* 1991; **34**(4/5):899–909.
8. Masmoudi W, Prat M. Heat and mass transfer between a porous medium and a parallel external flow. Application to drying of capillary porous materials. *International Journal of Heat and Mass Transfer* 1991; **34**(8):1975–1989.
9. Oliveira LS, Haghighi K. Conjugate/Adaptive finite element analysis of convective drying of porous media. *Proceedings of Ninth International Conference for Numerical Methods in Thermal Problems*, vol. IX, Atlanta, 1995; 80–88.
10. Nikitenko NI, Piyerskiy IM, Khomenko AS. Determination of stresses arising in drying of ceramic bodies. *Heat Transfer-Soviet Research* 1973; **5**:176–179.
11. Lewis RW, Strada MS, Comini G. Drying-induced stresses in porous bodies. *International Journal for Numerical Methods in Engineering* 1977; **11**:1175–1184.
12. Lewis RW, Morgan K, Thomas HR, Strada M. Drying-induced stresses in porous bodies—an elasto viscoplastic model. *Computational Methods in Applied Mechanics and Engineering* 1979; **20**:291–301.
13. Tsukada Takao, Sakai N, Hayakawa K. Computerized model of strain-stress analysis of food undergoing simultaneous heat and mass transfer. *Journal of Food Science* 1991; **56**:1438–1445.
14. Collard JM, Arnaud G, Fohr JP, Dragon A. The drying-induced deformations of a clay plate. *International Journal of Heat and Mass Transfer* 1992; **35**:1103–1115.
15. Ferguson WJ. A numerical prediction of the effect of airflow and wet bulb temperature on the stress development during convective wood drying. In *Mathematical Modelling and Numerical Techniques in Drying Technology*, Turner Ian, Majumdar AS (eds). Marcel Dekker Inc.: New York, U.S.A. 1997; 259–277.
16. Kowalski SJ, Musielak G, Rybicki A. The response of dried materials to drying conditions. *International Journal of Heat and Mass Transfer* 1997; **40**(5):1217–1226.
17. Segerlind LJ. *Applied Finite Element Analysis*. Wiley: Singapore, 1984.
18. Patnaik BSVP, Seetharamu KN, Aswatha Narayana PA. Simulation of laminar confined flow past a circular cylinder with integral wake splitter involving heat transfer. *Int. Num. Meth. Heat Fluid Flow* 1996; **6**:65–81.
19. Fortes Maruri, Okos MR. Heat and mass transfer in hygroscopic capillary extruded products. *A.I.Ch.E. Journal* 1981; **27**:255–262.
20. Zienkiewicz OC. *The Finite Element Method in Engineering Science*. McGraw-Hill: London, 1971.
21. Yang Chien-Tung, Atluri SN. An 'Assumed deviatoric stress-pressure-velocity' mixed finite element method for unsteady, convective, incompressible viscous flow: Part II: computational studies. *International Journal for Numerical Methods in Fluids* 1984; **4**:43–69.

